Paleomagnetism and Geochronology of the Southwestern Laurentia Large Igneous Province (SWLLIP)

Nicolas Anderson[1], Michael Mohr[2] Nicholas Swanson-Hysell[1], Yiming Zhang[1], Eben Blake Hodgin[1], Mark D. Schmitz[2]

[1] Department of Earth and Planetary Science, University of California, Berkeley, CA 94720, USA

[2] Department of Geoscience, Boise State University, Boise, ID 94720, USA

Keywords: Laurentia, LIP

Abstract

Late Mesoproterozoic mafic magmatism expressed as diabase sills, dikes, and rarely exposed flows between southeastern California and New Mexico is grouped as the Southwestern Laurentia large igneous province (SWLLIP). SWLLIP magmatism has been hypothesized to be the result of 1) lithospheric delamination after ca. 1140 Ma orogenesis; or 2) decompression melting of an upwelling mantle plume beneath Laurentia. One possible scenario is that an upwelling plume encountered topography at the base of Laurentian lithosphere, bifurcated and resulted in voluminous magmatic activity both in the SWLLIP and in the ca. 1108 to 1084 Ma Midcontinent Rift, ∼2000 km to the northeast. To test this hypothesis, it is crucial to obtain precise age constraints on the magmatism. Recent zircon U-Pb CA-ID-TIMS dates from the Midcontinent Rift in the Lake Superior region constrain the timing of voluminous pulses of magmatism, the largest being associated with rapid (<1 Ma) emplacement of the Duluth complex at ca. 1096 Ma. However, existing ages of SWLLIP sills are largely based on U-Pb baddeleyite dates that are discordant and lack sufficient precision and accuracy. In this work, we present new geochronological and paleomagnetic data on diabase sills that intruded the Crystal Springs Formation of the Death Valley region. Felsic segregations within some thick sills contain zircon which presents the opportunity to develop new high-precision CA-ID-TIMS $^{206}Pb/^{238}U$ dates. Paleomagnetic data from the sills provides additional insights on their age given that paleomagnetic poles can be compared to the well-dated Keweenawan Track of poles developed from the Midcontinent Rift. Our data constrain a pulse of sill emplacement in the Death Valley region ca. 1098 Ma slightly prior to the main stage of Midcontinent Rift magmatism. Simple analytical forward

modeling shows that lateral plume migration between the localities is plausible on such a short timescale.

Introduction

Large Igneous Provinces (LIPs) are typically short duration (<5 million year), voluminous (often >1 Mkm^3) intraplate magmatic events that are dominated by mafic magmas and typically attributed to the effects of upwelling mantle plumes (Ernst et al., a). The exact mechanisms of LIP generation are debated, likely not mutually exclusive, and range from 1) the arrival of a plume head (Campbell and Kerr) 2) edge-driven convection (Richards et al.), 3) lithospheric delamination (Tanton and Hager), 4) thermal anomalies due to changes in melt flow (Coltice et al.), 5) increased heat flow beneath super-continents (**?**) and/or 6) stagnation and hydration of a subducting slab at the mantle transition zone (MTZ) (van der Lee et al.). Seismic, petrologic and geochemical (Tsekhmistrenko et al.; Peters et al.; Herzberg and Gazel) evidence suggest that thermochemically distinct mantle plumes exist with many originating near the core-mantle boundary (French and Romanowicz) and initiate LIP melting upon their arrival at the base of the lithosphere (Richards et al.).

Large scale magmatism across the southwestern United States prior to, or coincident with, the *ca.* 1090 Ma onset of Rodinia assembly is grouped as the Southwestern Laurentia large igneous province (SWLLIP; Bright et al.). The SWLLIP spans the distance from southeastern California to northern Arizona to southeastern Arizona and is expressed as diabase sills and occasionally dikes and flows including the Cardenas Basalts and Unkar Sills of the Grand Canyon, Arizona (Fig. 1;Bright et al.). Exposed late Mesoproterozoic units in Death Valley, southern California chronicle the geological evolution of southwestern Laurentia and are essential for Rodinian paleogeographic reconstructions, as reconstructions typically place Laurentia at the core of the supercontinent (**?**St-Onge et al.; Whitmeyer and Karlstrom; Hoffman; Dalziel). Previously, Bright et al. compiled geochronology data from candidate units of the SWLLIP that involve techniques ranging from Ar/Ar and K/Ar thermochronology of biotite or whole rock, U-Pb thermal ionization mass spectrometry (TIMS) of zircon, baddeleyite and titanite, U-Pb sensitive high resolution ion microprobe (SHRIMP) of zircon and U-Pb laser ablation-inductively coupled plasma-mass spectrometry (LA-ICP-MS) of zircon. These data with variable precision and accuracy were interpreted to indicate a period of prolonged magmatic activity that spanned ∼123 million years from *ca.* 1163 to 1040

Ma (Bright et al.). However, considering that many of the data in the Bright et al. compilation have large uncertainties (often as much as a few tens of millions of years), an alternative interpretation is that they record multiple relatively short pulses of temporally distinguishable magmatism.

Bright et al. also noted that the timing of the SWLLIP magmatism and that of the ca. 1.1 Ga North American Midcontinent Rift (MCR) could have a substantial overlap, leading them to propose a comagmatic relationship in which an upwelling plume bifurcated upon encountering topography at the base of the lithosphere and laterally migrated toward both SWLLIP and the MCR (Fig. 1, 14). This hypothesis would predict fast-moving plume branches that would result in magmatism in the two regions that are only a few million years apart despite their large spatial separation (∼2400 km; Fig. 1; Sleep). Though Bright et al. proposed this hypothesis, the U-Pb baddeleyite (zirconium oxide) TIMS ages they obtained in their study for SWLLIP are far too young (ca. 1080 ±3 Ma, 1088 ±3 Ma and 1094 ±2 Ma) to be related to ca. 1.1 Ga Midcontinent Rift magmatism, as the events need to occur within a few million years of each other. To evaluate the bifurcating plume and lateral magma migration hypothesis, high-precision geochronological constraints are needed on units in both regions. However, previous geochronology data of SWLLIP lack sufficient temporal resolution in comparison to the well-dated Midcontinent Rift units that typically have age uncertainties within 500 kyrs (Swanson-Hysell et al., b). Pioneering U-Pb geochronology work on SWLLIP units more roughly constrain their ages than is possible with previous methods. Baddeleyite U-Pb methods or laser-ablation techniques often yield discordant ages due to the difficulty of mitigating Pb loss. In addition, the current compilation is dominated by felsic units as zircons tend to be more abundant in felsic lithologies than in mafic ones (Bright et al.).

Modern chemical abrasion isotope dilution-thermal ionization mass spectrometry (CA-ID-TIMS) U-Pb geochronology produces high-precision $^{206}Pb/^{238}U$ dates from chemically abraded zircon crystals (Mattinson). These $^{206}Pb/^{238}U$ dates are also considered to be more accurate than systematically older $^{207}Pb/^{206}Pb$ dates (Schoene; Schoene et al.). CA-ID-TIMS geochronology of zircon has the resolution to distinguish magmatic pulses on the scale of <1 m.y. and can provide insight into timing and tempo of rapid magmatism of large igneous provinces (**?**Swanson-Hysell et al., b). Despite mafic lithologies typically forming under silicon-undersaturated conditions that favor baddeleyite crystallization over zircon precipitation, zircon-saturated felsic segregation can occur within thick mafic bodies (**?**)e.g.>Bleeker2006. In this study, we present new high-precision $^{207}Pb/^{206}Pb$ zircon dates from three thick diabase sills from

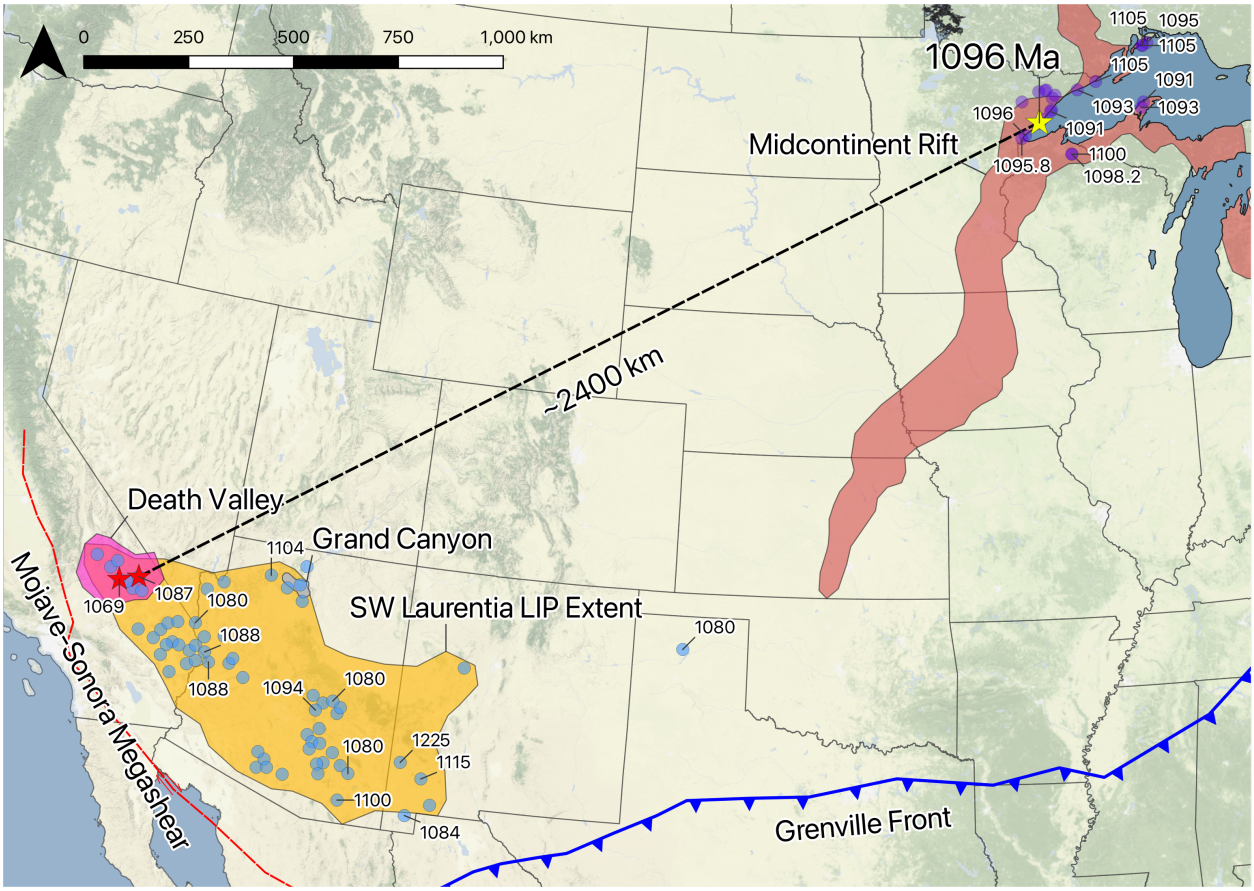

Figure 1. Simplified map illustrating the positions of the mafic sills (blue) interpreted to be associated with SWLLIP as mapped in a compilation by Bright et al. (2014). Ages span ~123 million years from 1163 Ma to 1040 Ma. Shown in purple are recent CA-ID-TIMS dates from Midcontinent Rift magmatic events that span 22 Ma from 1105 - 1083 Ma. The red stars highlight previous discordant geochronology in Death Valley from (Heaman and Grotzinger). The yellow star highlights a massive pulse of magmatism at ca. 1906 Ma associated with the emplacement of the Duluth Complex of the Midcontinent Rift. The Duluth complex is the second largest mafic intrusive complex on earth (Swanson-Hysell et al., a)

Death Valley, CA, to constrain the timing of the magmatism in the region.

Paleomagnetic data can provide additional age constraints on rocks from which precise absolute geochronology data is difficult to obtain such as mafic sills without felsic segregations. Laurentia experienced a period of rapid latitudinal plate motion during rift development Swanson-Hysell et al. (b). A synthesized apparent polar wander path (APWP) based on the Midcontinent Rift volcanic rocks indicates that motion exceeded 20 cm/yr Swanson-Hysell et al. (b), faster than the maximum speed of India of ~17 cm/yr during the Cenozoic in the lead-up to its collision with Euraisa **?**. This motion resulted in significant differences in pole positions recorded by Midcontinent Rift rocks that were emplaced a few million years apart Swanson-Hysell et al. (b). In this study, we develop paleomagnetic data from the Mesoproterozoic

mafic sills in Death Valley to accompany the zircon geochronology data. Our results better constrain the timing of SWLLIP diabase sill emplacement, refine current Death valley chronostratigraphy and allow for the testing of the bifurcating plume and lateral magma migration model.

1 Pahrump Group Stratigraphy

Tectonism and erosion within the Mojave has exposed ∼1.5 - 4 meters of Meso-Neoproterozoic sedimentary rocks of the Pahrump Group (Crystal Springs-Horse Thief Springs-Beck Springs-Kingston Peak Formations; Fig. 4) within the basin and range province, that are interpreted to have been deposited in extensional basins in response to long-term rifting of Rodinia, just prior to Snowball Earth(Macdonald et al.; Smith et al.). The Pahrump Group sits atop a metamorphosed basal unit of granitic gneiss and quartz monzonite dated *ca.* 1780 - 1400 Ma. An unconformity of ∼300 Ma delineates the basement from the overlying strata of the Crystal Springs Formation Fig. 4 (Strickland et al.; Barth et al.; Labotka et al.).

1.1 Crystal Springs Formation

The Crystal Springs Formation is a ∼750 thick sequence of marine deposits ranging from siliciclastic to carbonate-dominated Smith et al.; Prave. The formation can be separated into six units, from oldest to youngest: Arkosic sandstone Member, Feldspathic Sandstone Member, Argillic mudstone Member, Dolomite Member, Algal Member and Chert Member (Macdonald et al.). The Arkose Member is characterized by interbedded sandstone and conglomerate whose coarse grained units display trough cross-bedding which grades to planar, tidal cross-bedding in the finer grained units. The Feldspathic Sandstone Member exhibits cyclical sequences of red sandstone, siltstone and shale, textured with tidal crossbedding, mudcracks and ripple cross-lamination. Massive weathered purple Argillite with reduction spots dominate the Mudstone Member (Smith et al., 2016). These lower three members are interpreted as facies changes from a south-flowing fluvial system to an intertidal-deltaic system with a southern source (Macdonald et al.; Roberts, a,b). The cherty-dolomite unit rests above the purple argillited and is distinguished by cross stratified and often brecciated cyclically bedded dolomite/dolomitic limestone and wavy-bedded cherty-dolomite, interpreted to represent a high energy intertidal zone (Macdonald et al.; Wrucke).

1.1.1 Diabase Sills

∼90 - 120 m thick sills of diabase intrude the Crystal Springs Formation above and below the cherty dolomite member. The diabase is dark-green to greenish-black and often grade from medium-grained to course-grained at center of the sill. The sill textures are generally diabasic but an occasional irregularly shaped calcic plagioclase porphoritic texture can be observed at sill margins (Wright) (Fig. **??**).

50-80% of the sills have experienced pervasive dueteric alteration but pseudomorphs and relict primary minerals imply an original mineral assemblage of hornblende, actinolite, plagioclase, epidote, sericite, green and brown biotite and chlorite.(Hammond).

1.1.2 Talc-Tremolite Zones

Talc-tremolite bearing zones are produced during contact metamorphism when intruding sills heat magnesium and silica rich groundwater allowing for replacement interactions within the cherty-dolomite member (Wright). Talc-tremolite metamorphism exists within a ∼30 m thick metamorphic zone adjacent to sill margins (Wrucke; Heaman and Grotzinger; Wright). Siliceous cherty dolomite is highly sensitive to thermal metamorphism and the absence of metamorphic minerals other than talc indicate that metamorphism did not take place in an open system where CO2 could be degassed during formation of calcium-magnesium silicate minerals. Metamorphic minerals would not have developed beyond an initial stage, and late-aqueous solutions concentrated in magnesium and silica would be available for alteration of the diabase and cherty dolomite to produce talc (Wrucke).

Talc formation in the host rocks of the Crystal Springs Formation is assumed to have occured "early on during sill emplacement" [quantify time better] from deuteric hydrothermal alteration in sill fracture zones ().

The Stromatalitic Member is identified by cyclic stramatolitic limestone and contains the second expression of Crystal Springs diabase sills (**?**)

Within eastern Warm Springs Canyon 6 sills are particularly well exposed (Warm Springs Canyon Map, Fig. 6). A sill that has intruded another sill can be found on the southside of Warm Springs Canyon near the now defunct Grantham Mine and is identified by fine-grained chilled contacts within the younger sill

(CS5) against the coarse-grained center of the host sill (CS6) (Fig: 2). Even at variable stratigraphic heights, many of the exposed sills are interconnected suggesting most were emplacement from a single magmatic injection. However, the intrusion of CS5 sill into the CS6 sill indicates at least one subsequent magmatic episode. (Wrucke)

Figure 2. Photo depicting the contact between the younger fine-grained intrusive inner sill (CS5) and the older coarse-grained outer sill.

Previous radiometric diabase age constraints for Death Valley diabase sills were obtained from U-Pb TIMS analysis of discordant multigrain baddeleyite samples obtained from 2 sills, with ages interpreted from their upper intercepts with the concordia. A sill in the Kingston Range dated in Heaman and Grotzinger had multi-grain fractions that were ∼3-9% discordant and had an upper intercept of 1087 ±3 Ma. A sill dated at Saratoga Springs had dated fractions that were ∼11 to 19% discordant and had an upper intercept of 1069 ±3 Ma. It is interpreted that the discordance of the baddeleyite grains is likely from Pb loss or due to younger sporadic botryoidal zircon growth found coating the grains, likely from recent, low-temperature fluid interactions (Heaman and Grotzinger).

1.2 Horse Thief Spring and Beck Spring Formation

An up to 20^{o} angular erosional unconformity separates the upper chert member of Crystal Springs from the overlying mixed carbonate-siliclastic units of the *ca.* 770 Ma Horse Thief Spring (formerly Upper Crystal Springs Formation) and Beck Spring Dolomite Formations (Mahon et al.; **?**). In some localities, the unconformity corresponds with a 0-30 m thick hornfelsic breccia unit (Mahon et al.). The presence of

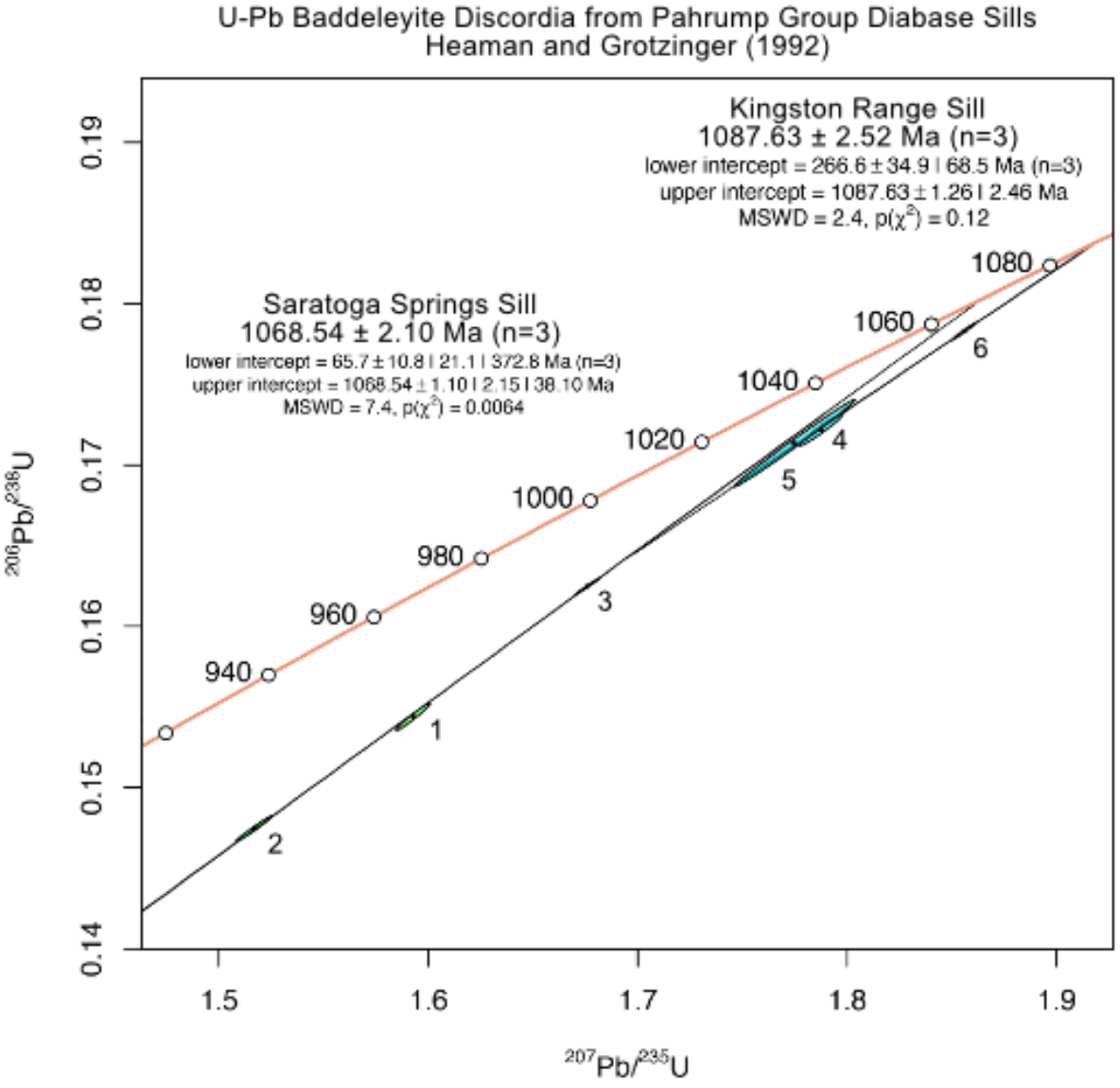

Figure 3. Concordia comparison between concordant *ca.* ∼1098 Ma zircon bearing felsic segregation samples F20205, CS4 and CS7 obtained in this study. Previously dated discordant Death Valley baddeleyite are shown. Upper intercepts from 1992 study of Saratoga Springs Sill and Kingston Range sill are 1069 ±3 Ma and 1087 ±3 Ma, respectively (Heaman and Grotzinger).

dolomitic microbialite, mixed carbonate and siliciclastics, in conjunction with silt, sand and pebble conglomerates within the Horse Thief and Beck Springs Formations capture a change in sediment provenance within the basin from NE (in the Crystal Springs) to SW. (Smith et al.) and (Macdonald et al.)

158 argue that the provenance change indicates 2 separate basin forming events, in which the Crystal Springs
159 Formation was deposited on a south facing open margin, followed by an uplift during basin inversion,
160 allowing for the Horse Thief Spring and Beck Spring Formation to deposit on a north facing margin.

161 1.3 Kingston Peak Formation

162 Another unconformity marks the transition from Beck Spring Dolomite to the overlying Kingston Peak
163 Formation, the uppermost unit of the Pahrump Group. The Kingston Peak Formation is known for
164 massive glacial diamictites, dropstones, and striated clasts linked to Cryogenian deposition during the
165 Sturtian Snowball Earth (ca. 717 to 660 Ma; (Smith et al.; Macdonald et al.).

166 1.4 Noonday Formation

167 Resting unconformably above the Kingston Peak Formation is the ca. 635 Ma Noonday Formation which is
168 followed by the Johnnie Formation. Within the sample localities there is significant variability of the units
169 present; see location specific geologic maps for greater detail.

170 Crystal Springs Stratigraphy

171 1.5 Diabase

172 2 Methods and Results

173 2.1 Zircon Geochronology

174 Three samples of zircon-bearing felsic segregations were collected for U-Pb CA-ID-TIMS geochronology. 2
175 of the samples are from distinct sills in Warm Springs Canyon (F20205 and CS4, Fig. 6) and 1 site from a
176 sill in the Central Ibex range (sill CS7; Fig. 7). Grain size within the diabase sills grades from very fine
177 near the contact with strata of the Crystal Springs Formation to up to 1 cm toward the sill interior. In the
178 interior, sill CS4 and CS7 contain felsic melt segregations that were injected as dikelets and sillets that are

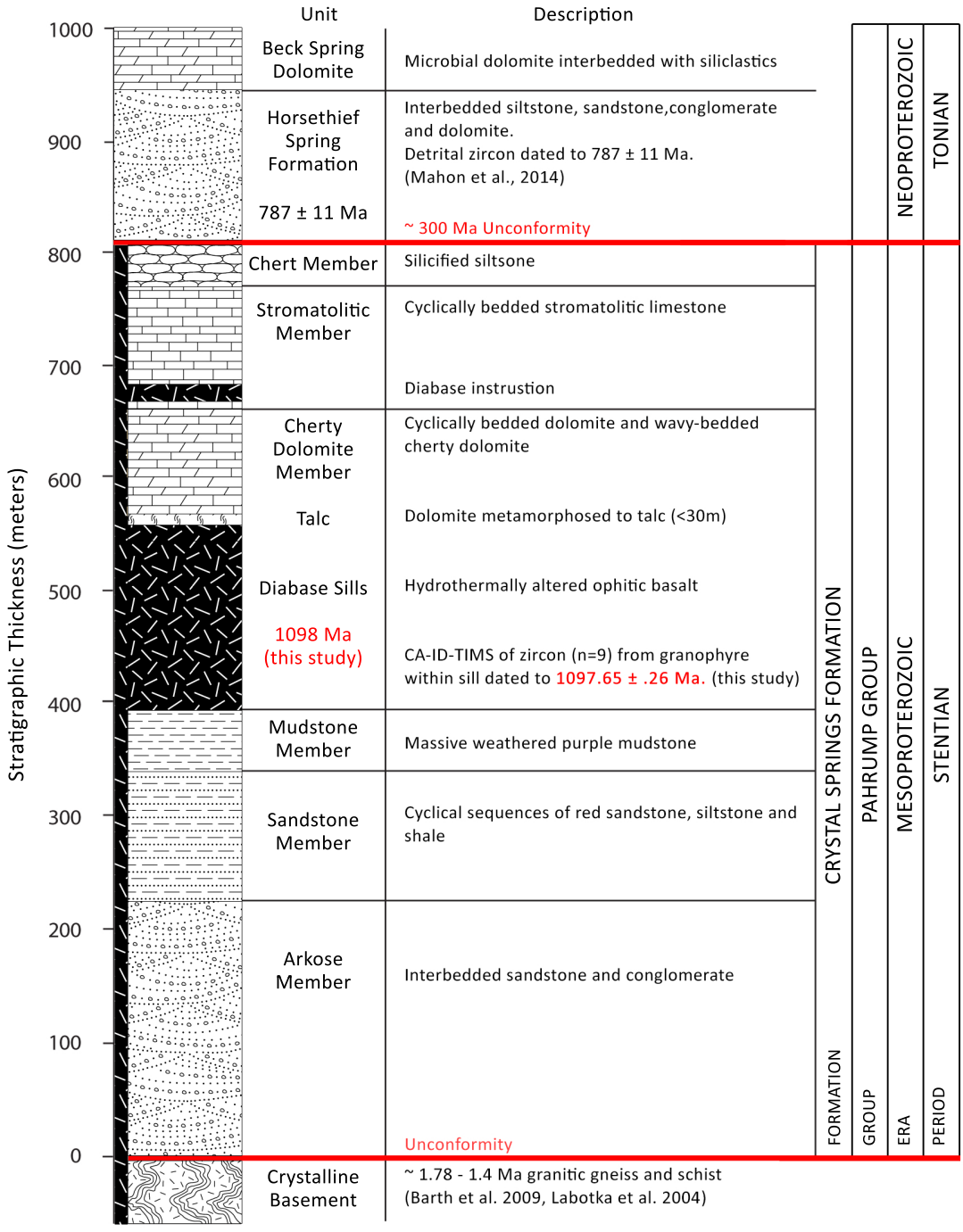

Figure 4. Generalized stratigraphy of the Crystal Springs Formation modified from (Macdonald et al.; Roberts, a)

bulbous to planar in geometry. This minor silicic melt represents the late-stage differentiation of mafic magma and record sill crystallization age. Sills exposed in Death Valley are sufficiently thick (sill size) to

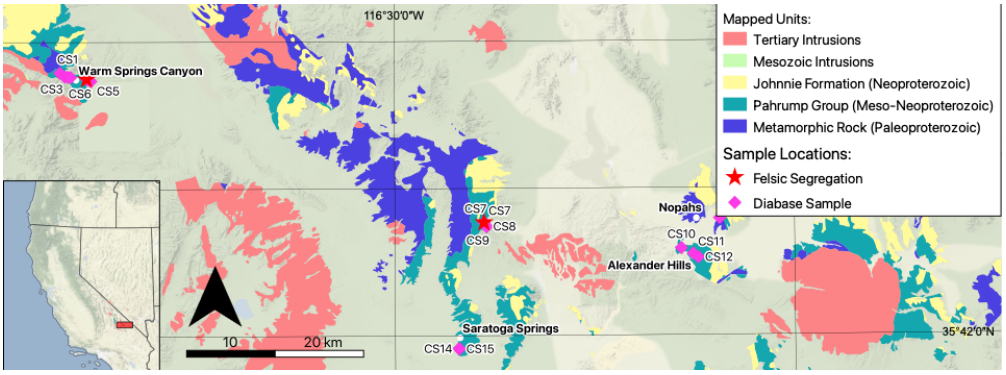

Figure 5. Geologic map of southern Death Valley, California, USA. The map highlights diabase sites sampled for paleomagnetic study and samples of late stage felsic melt segregations collected within diabase sills for geochronology, as well as relevant Proterozoic geological units, and recent intrusions. Sample locations that yielded U-Pb dates obtained from felsic intrusion samples in Warm Springs Canyon and the central Ibex Range are indicated by red stars. The Crystal Springs (CS) Formation of the Pahrump Group is host to majority of the Southwestern Laurentia large igneous province (SWLLIP) diabase sills and dikes in the region. Paleomagnetic sample sites CS1-6 were collected in southern Warm Springs Canyon; CS7-9 in the central Ibex Range; CS10-12 in the northern Alexander Hills; CS13 in the eastern Nopah Range; CS14-15 in southern Saratoga Hills. Extent of geologic units modified after Workman et al. (2002), USGS Field Studies Map MF-2381.

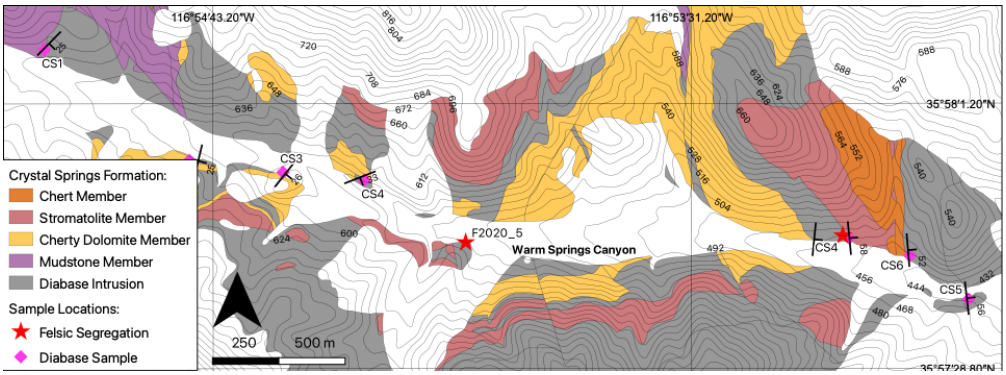

Figure 6. Geologic map of southern Warm Springs Canyon detailing Crystal Springs geochronology (red star) and paleomagnetic sites (pink diamond) CS1-6 and lithological units of the Pahrump group. Within the Pahrump Group, the Crystal Springs Formation sits atop metamorphosed crystalline basement rock and is capped unconformably by the Noonday Formation. U-Pb dates were obtained from zircon bearing felsic segregations found at CS4 and $F2020_5$, $indicated by red stars. Note: paleomagnetic sample CS4 and geochronology sample G1 are from the same diabase sill.$

fractionate melt pockets with a high enough silica content to entrain zircons.

Zircons were separated from bulk samples of the felsic segregation using panning and heavy liquid mineral separation methods. 21 zircons from 3 sills (F20205, n=8; CS4, n=9; CS7, n=7) were chemically abraided in hydrofluoric (HF) acid and analyzed using isotope dilution–thermal ionization mass spectrometry (ID-TIMS) in the Boise State Isotope Geology Laboratory using EARTHTIME tracer solutions (Condon et al.).

Zircons obtained from 3 sills yielded precise, indistinguishable $^{206}Pb/^{238}U$ dates with overlapping

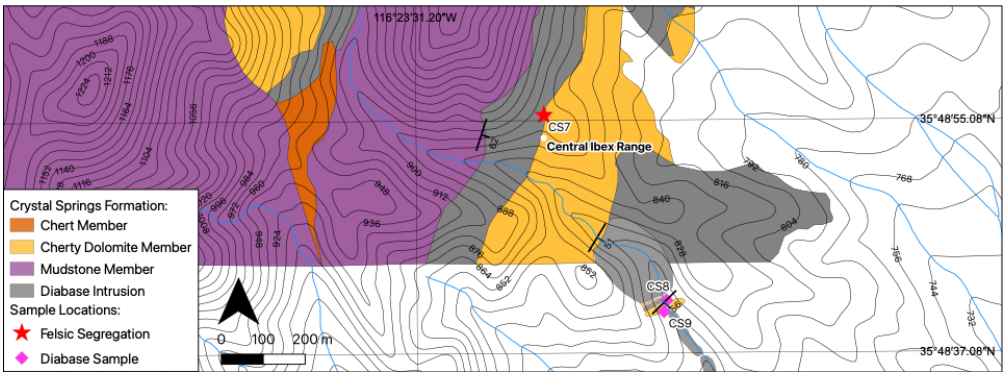

Figure 7. Geologic map of Central Ibex Hills highlighting Crystal Springs paleomagnetic and geochronology sites CS7-9, as well as exposed units of the Crystal Springs Formation.

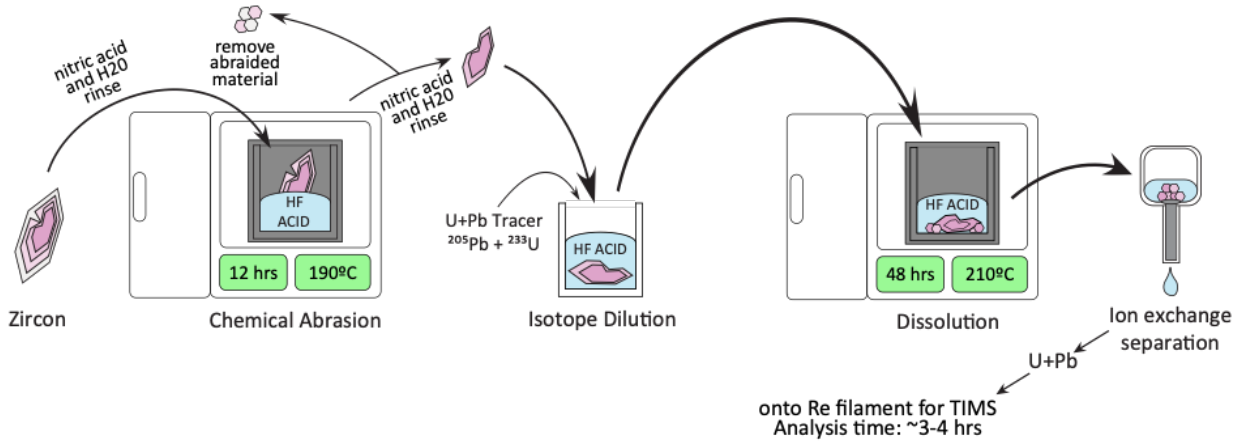

Figure 8. Following thermal annealing, single grains of zircon are chemically abraded in hydrofluoric acid at 190°C for 12 hrs to radiation damaged zones of the zircon that may have experienced lead loss. Abraded material is thrown out and zircon is then spiked with a known ratio of synthetic $^{2}05Pb/^{2}33U$ which is used as a calibration tracer. Spiked zircon solution is placed back into the oven for 48 hours at 220°C until completely dissolved. Dissolved solution is passed through resin to separate out only uranium and lead. Final zircon sample is added to silica gel and placed on an Re filament for TIMS analysis. Figure modified from Schoene et al..

uncertainties (2σ). The weighted mean ages are 1097.91 ±0.29 Ma for site F20205, 1098.27 ±0.27 Ma for site CS4 and 1098.09 ±0.91 Ma for site CS7. Weighted means were calculated using multiple $^{206}Pb/^{238}U$ dates from single zircons (Table 1). Analytical, tracer and decay uncertainties and mean squared weighted deviation (MSWD) are reported in (Table 1) and Fig. 9.

These dates tightly constrain the crystallization ages of these three Death Valley diabase sills to ca. 1098 Ma and provides a minimum depositional age for the sediments of the Crystal Springs Formation.

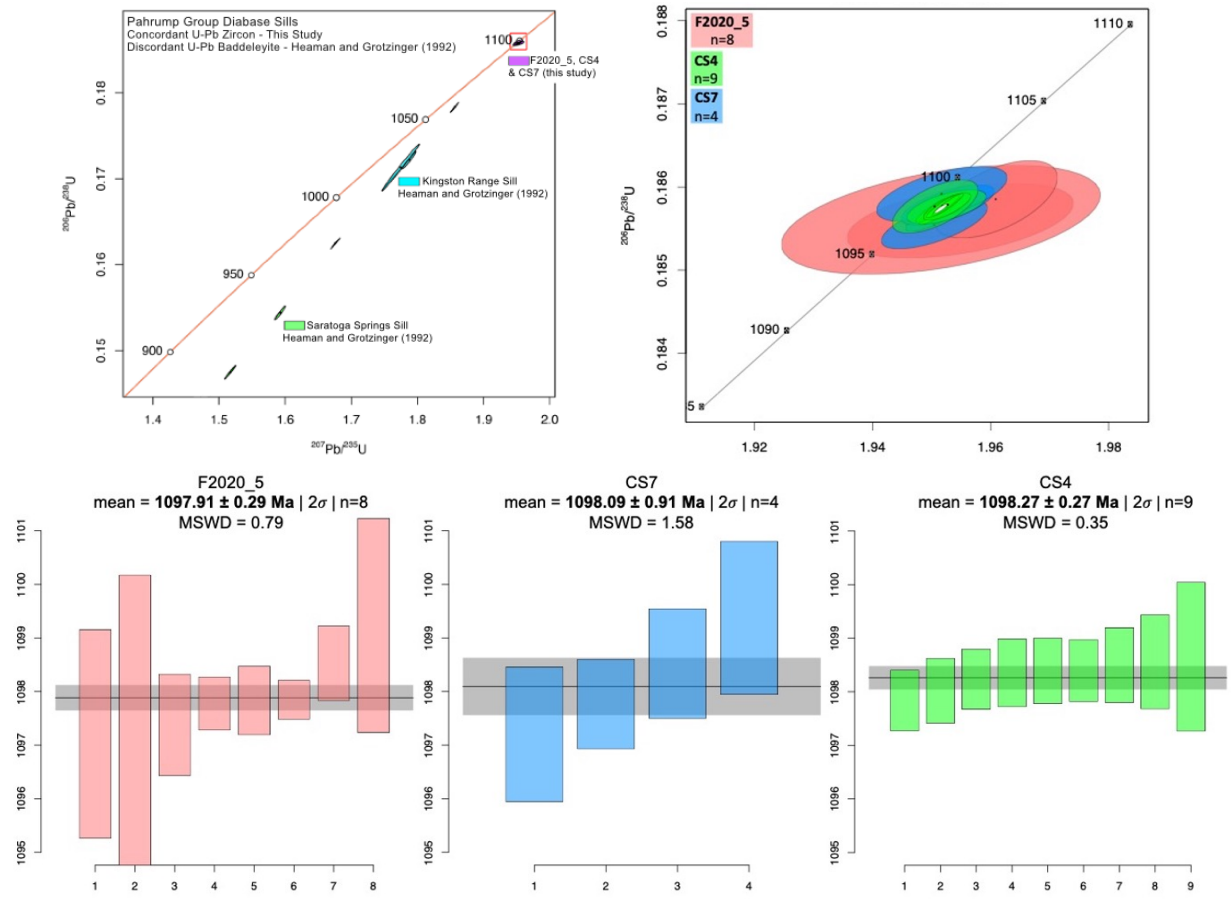
Pahrump Group Diabase Sills
Concordant U-Pb Zircon - This Study
Discordant U-Pb Baddeleyite - Heaman and Grotzinger (1992)
F2020_5, CS4 & CS7 (this study)
Kingston Range Sill Heaman and Grotzinger (1992)
Saratoga Springs Sill Heaman and Grotzinger (1992)
F2020_5 n=8
CS4 n=9
CS7 n=4
F2020_5 mean = 1097.91 ± 0.29 Ma | 2σ | n=8 MSWD = 0.79
CS7 mean = 1098.09 ± 0.91 Ma | 2σ | n=4 MSWD = 1.58
CS4 mean = 1098.27 ± 0.27 Ma | 2σ | n=9 MSWD = 0.35

Figure 9. U-Pb zircon CA-ID-TIMS data from felsic segregations samples F20205, CS4 and CS7. **Top Left:** Concordia diagram showing concordance between $^{206}Pb/^{238}Pb$ and $^{207}Pb/^{235}Pb$ systems indicating *ca.* ∼1098 Ma. **Top Right:** Ranked age plot for 9 zircons with a weighted mean distribution of 1097.57 ±.26 Ma obtained from $^{207}Pb/^{207}Pb$ ratios. **Bottom:** Plots generated using IsoplotR (Vermeesch)

2.2 Paleomagnetism

A total of XXX distinct diabase sill were sampled for paleomagnetic study. For each site 2.5 cm diameter paleomagnetic cores where extracted from mafic rock using a gasoline powered diamond tipped drill and oriented using both magnetic and sun compasses (when possible). Sample azimuths were preferentially determined using sun compass orientations. Sampled cores were taken from 2 diabase sills exposed within the the units of the Crystal Springs Formation of the Pahrump Group. The five localities where cores were obtained are plotted in Fig. **??**. 7-10 samples were collected for 15 sites of diabase across ∼80 km of Death Valley. 7 sites were collected as whole rock block samples due to drilling regulations within Death Valley National Park. Exposed face of block samples were oriented with brunton compass and sun compass when

possible. In the laboratory the block samples were reoriented to their original in situ positions. Drill cores from the blocks were oriented using a Pomeroy magnetic compass.

Once all cores were extracted, the samples were cut and prepared into 1.5 cm tall cylinders for analysis on a 2G Enterprises DC-SQUID superconducting rock magnetometer with an automated sample changing system. Natural remnant magnetization (NRM) was measured for all samples followed by step-wise thermal demagnetization in a magnetically shielded room at the UC Berkeley Paleomagnetic Lab. Temperature intervals are reduced from 100ºC to 5ºC as temperature approaches 540°C - 585°C and 670°C - 685°C, dependent on the suspected magnetic carrier. The magnetic field in the shielded room is <500 nT and the field within the demagnetizing chamber is <10 nT. The quartz glass sample holder has a typical magnetic moment of 5 x 10^{-12} Am^2. The PmagPy software package was used for least-square fits for principal component analysis of specimen demagnetization data (Tauxe et al.). Virtual geomagnetic poles, and α_{95} uncertainity ellipses were calculated using Fisher statistics.

The diabase demagnetization principal component analysis shows that origin trending characteristic remnant magnetization (ChRM) can often be isolated after the removal of a more recently acquired secondary component, during the first low temperature demagnetization steps up to 300°C (Fig. 10). ChRMs typically unblock during demagnetization steps ∼500°C to ∼580°C, consistent with titanomagnetite and magnetite as the primary carriers of remnant magnetization. Primary remnant magnetization is interpreted to have been acquired during diabase sill emplacement and cooling.

Site mean paleomagnetic directions are presented in (Table XXX). Thermal demagnetization without an alternating field is effective in removing secondary components and isolating single vector primary ChRM. A virtual geomagnetic pole was calculated for each site sampled.

Obtained paleomagnetic directions were tilt-corrected back to paleohorizontal to ensure developed paleomagnetic poles accuracy for comparison to Laurentia's apparent polar wander path (APWP; fig (Swanson-Hysell et al., b)). The structural orientation of the SWLLIP sills can be determined using bedding orientations from basal bedding units and adjacent sills.

Tilt corrected ChRMs in 4 out of a total of 15 (CS1, CS2, CS6 and CS8) diabase sill samples display a W-NW declination with a moderate downward inclination with good consistency between specimen and site level measurements. The tilt-corrected mean pole of the 4 sites (lat lon n a95 k) are plotted against an

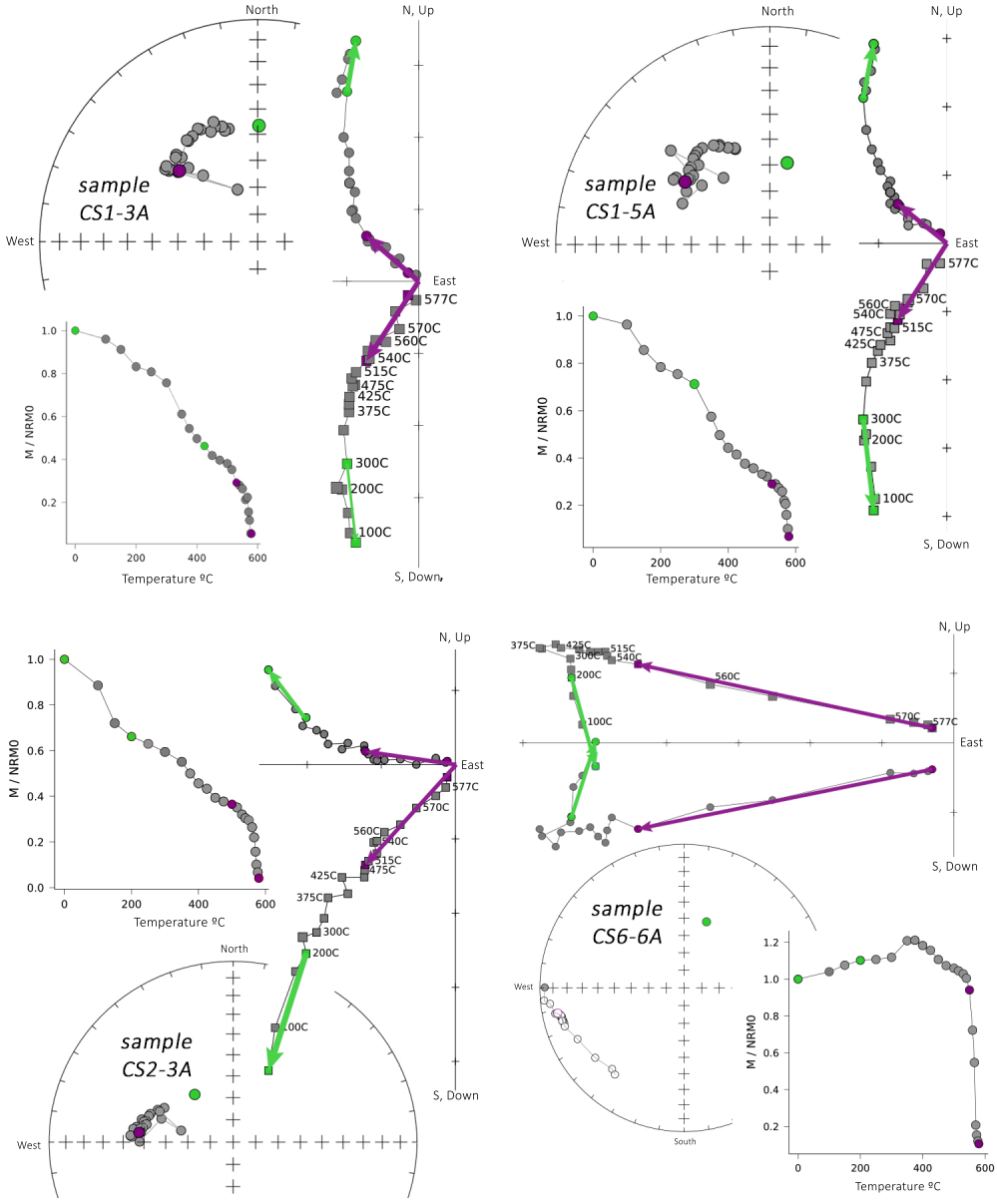

Figure 10. Representative orthogonal vector demagnetization diagrams for Crystal Springs diabase specimens. Thermal demagnetization steps decay of characteristic remnant magnetizations (ChRM) (purple) toward the origin after removal of secondary components. (green). ChRM directions between the sites show distinct W-NW trend with a moderate inclination. Magnetization versus demagnetization stepwise heating plots are paired with orthogonal vector plots and equal area plots of paleomagnetic directions. Representative Zijderveld, equal area and demagnetization plots for reliable paleomagnetic samples. The steep northerly component (green) was removed during thermal demagnetization (up to ∼300°C) and is interpreted as the present-day local field (PLF) overprint. The demagnetization shoulder at ∼360°C is consistent with pyrrhotite presence. Steep drop in magnetization at ∼580°C is indicative of magnetite as dominant high temperature magnetic carrier. Zijderveld plot shows expected W-NW declination with a moderate downward inclination, held by magnetite (purple).

231 APWP synthesized from Midcontinent Rift volcanics that show the mean specimen and site pole plotting

232 at the expected pole position for a date of *ca.* 1098 Ma (fig). Three sills contained...

233 This mean pole position are consistent with the expected date of ∼1098 Ma

234 dates obtained from zircon geochronology and may support coeval magmatic activity between SWLLIP
235 and the Midcontinent Rift.

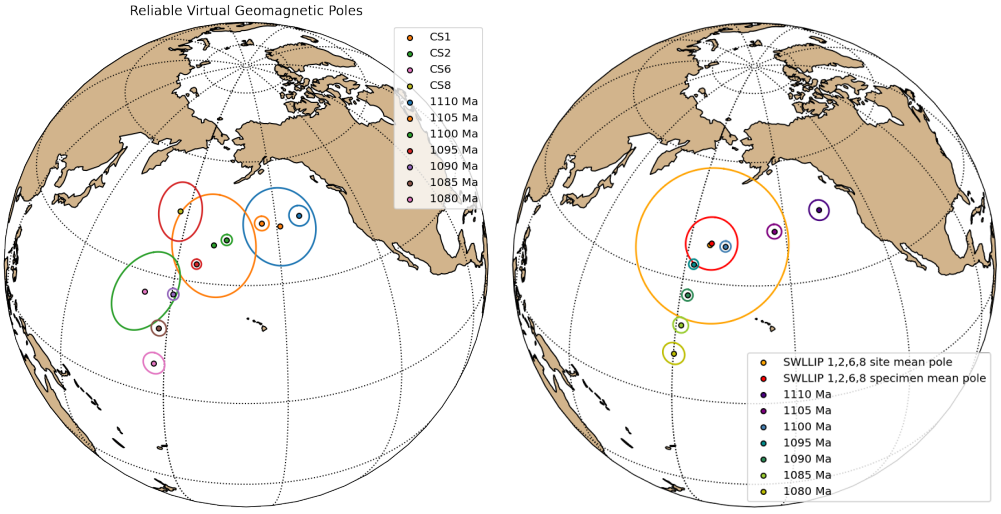

Figure 11. Left: Tilt-corrected virtual geomagnetic poles (VGPs) for 4 sites (CS 1,2,6,8) of SWLLIP diabase with 95% confidence angle $_{95}$ <15[a] site mean paleomagnetic directions give mean poles of: 1 2 3 4; where k is Fischer's precision parameter. Right: Specimen and site level means plotted against Midcontinent Rift pole path synthesized from volcanic poles.

236 # Discussion

237 ## MCR date comparison, Lubrication theory, Upwelling Plume and Lateral
238 ## Spread

239 It is estimated greater than xxxx km^3 of lava erupted from the SWLLIP in less than 1 million years. The
240 xxx meter thick diabase sills and dykes represent flows of mildly alkaline basaltic composition derived from
241 an enriched mantle source (Shirey; Nicholson and Shirey; Hammond). SWLLIP magmatism is attributed
242 to decompression melting of an upwelling mantle plume and lithospheric extension above the plume
243 location (Hutchinson et al.). Magmatism in the area has previously been reported as a LIP due to the
244 mafic composition, spatial extent and intraplate location within an extensional regime (Ernst and Buchan;
245 Ernst et al., b; Conway et al.; **?**; **?**). The occurrence of Widespread horizontal sheets a The occurrence of

SWLLIP at a time when widespread voluminous magmatism was prevalent across Laurentia, specifically at the MCR, reinforces the interpretation that the events were coeval and plume related. The presence of silicic melts, felsic segregations, in the innermost interior of mafic sills exposed in Death Valley is consistent with 1) the tail end of a mantle plume or 2) the partial melting of the lower crust from underplating of mafic magma, possibly associated with a stagnant subducted slab beneath Laurentia (Bryan and Ferrari; Ernst et al., b).

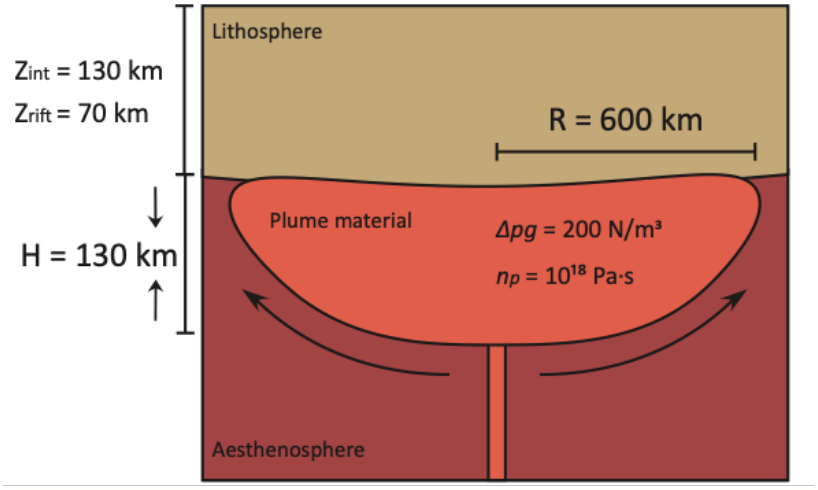

Figure 12. caption

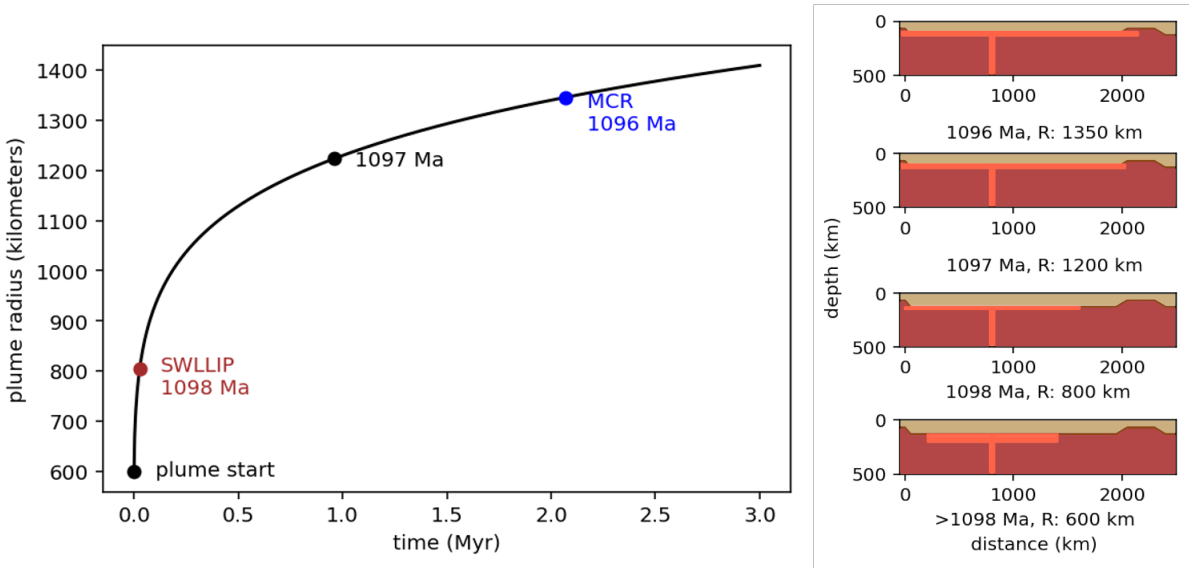

Figure 13. Increasing plume radius with respect to time for a plume head with a height of 130 km and a width 600 km demonstrating a possible 2 Ma travel time for lateral magma migration between SWLLIP and the MCR.

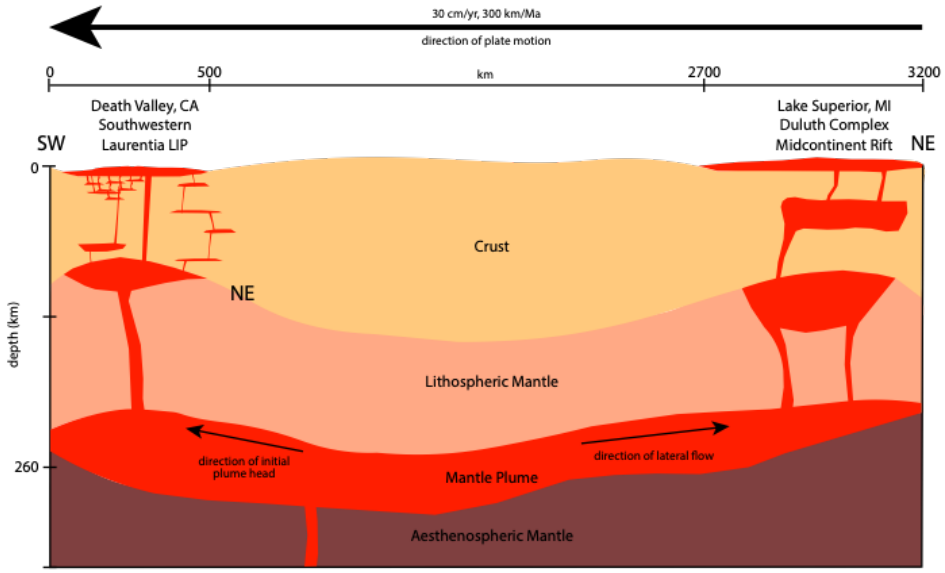

Figure 14. Schematic cross section of Laurentia ca. 1100 Ma. Possible bifurcating plume model is based on Bright et al. (2014). An upwelling magma plume encounters the base of the fast moving Laurentian lithosphere and then radiates outward laterally. Lateral flow may be constrained rheologically to the NE by the Wyoming craton to the northwest and the xxx terrane to the southeast (**??**). Geochronology and modelling support SWLLIP emplacement at *ca.* 1098 Ma followed by a lateral magma migration ∼2300 km to the northeast, emplacing the Duluth Complex of the Midcontinent Rift at *ca.* 1096 Ma. Shearing between lithosphere and upper mantle may have produced higher temperatures and sustained effusive flow into the Midcontinent Rift. add volume to mantle plume and correct MCR diameter

References

Barth, A., Wooden, J., Coleman, D., and Vogel, M., , Assembling and disassembling california: A zircon and monazite geochronologic framework for proterozoic crustal evolution in southern california: vol. 117, pp. 221–239, doi:10.1086/597515.

Bright, R. M., Amato, J. M., Denyszyn, S. W., and Ernst, R. E., , U-pb geochronology of 1.1 ga diabase in the southwestern united states: Testing models for the origin of a post-grenville large igneous province: vol. 6, pp. 135–156, doi:10.1130/L335.1.

Bryan, S. E. and Ferrari, L., , Large igneous provinces and silicic large igneous provinces: Progress in our understanding over the last 25 years: vol. 125, pp. 1053–1078, doi:10.1130/B30820.1.

Campbell, I. H. and Kerr, A. C., , The great plume debate: Testing the plume theory: vol. 241, pp. 149–152, doi:10.1016/j.chemgeo.2007.01.013.

Coltice, N., Phillips, B., Bertrand, H., Ricard, Y., and Rey, P., , Global warming of the mantle at the origin of flood basalts over supercontinents: vol. 35, p. 391, doi:10.1130/G23240A.1.

Condon, D., Schoene, B., McLean, N., Bowring, S., and Parrish, R., , Metrology and traceability of u–pb isotope dilution geochronology (EARTHTIME tracer calibration part i): vol. 164, pp. 464–480, doi:10.1016/j.gca.2015.05.026.

Conway, C., Condie, K., and Noll, P., , Geochemical and detrital mode evidence for two sources of early proterozoic sedimentary rocks from the tonto basin supergroup, central arizona—reply: vol. 87, pp. 241–244, doi:10.1016/0037-0738(93)90007-R.

Dalziel, I. W., , Pacific margins of laurentia and east antarctica-australia as a conjugate rift pair: Evidence and implications for an eocambrian supercontinent: vol. 19, p. 598, doi:10.1130/0091-7613(1991)019<0598:PMOLAE>2.3.CO;2.

Ernst, R., Liikane, D., Jowitt, S., Buchan, K., and Blanchard, J., a, A new plumbing system framework for mantle plume-related continental large igneous provinces and their mafic-ultramafic intrusions: vol. 384, pp. 75–84, doi:10.1016/j.jvolgeores.2019.07.007.

Ernst, R., Wingate, M., Buchan, K., and Li, Z., b, Global record of 1600–700ma large igneous provinces (LIPs): Implications for the reconstruction of the proposed nuna (columbia) and rodinia supercontinents: vol. 160, pp. 159–178, doi:10.1016/j.precamres.2007.04.019.

Ernst, R. E. and Buchan, K. L., , Large mafic magmatic events through time and links to mantle-plume heads, Geological Society of America: doi:10.1130/0-8137-2352-3.483, URL https://pubs.geoscienceworld.org/books/book/518/chapter/3801296.

French, S. W. and Romanowicz, B., , Broad plumes rooted at the base of the earth's mantle beneath major hotspots: vol. 525, pp. 95–99, doi:10.1038/nature14876.

Hammond, J. G., , Geochemistry and petrogenesis of proterozoic diabase in the southern death valley region of california: vol. 93, pp. 312–321, doi:10.1007/BF00389390.

Heaman, L. M. and Grotzinger, J. P., , 1.08 ga diabase sills in the pahrump group, california: Implications for development of the cordilleran miogeocline: vol. 20, p. 637, doi:10.1130/0091-7613(1992)020<0637:GDSITP>2.3.CO;2.

Herzberg, C. and Gazel, E., , Petrological evidence for secular cooling in mantle plumes: vol. 458, pp. 619–622, doi:10.1038/nature07857.

Hiess, J., Condon, D. J., McLean, N., and Noble, S. R., , 238u/235u systematics in terrestrial u-bearing minerals: p. 49.

Hoffman, P. F., , Did the breakout of laurentia turn gondwanaland inside-out?: vol. 252, pp. 1409–1412.

Hutchinson, D. R., White, R. S., Cannon, W. F., and Schulz, K. J., , Keweenaw hot spot: Geophysical evidence for a 1.1 ga mantle plume beneath the midcontinent rift system: vol. 95, p. 10,869, doi:10.1029/JB095iB07p10869.

Labotka, T. C., Albee, A. L., Lanphere, M. A., and McDowell, S. D., , Stratigraphy, structure, and metamorphism in the central panamint mountains (telescope peak quadrangle), death valley area, california: vol. 91, pp. 843–933, doi:10.1130/GSAB-P2-91-843.

Macdonald, F. A., Prave, A. R., Petterson, R., Smith, E. F., Pruss, S. B., Oates, K., Waechter, F., Trotzuk, D., and Fallick, A. E., , The laurentian record of neoproterozoic glaciation, tectonism, and eukaryotic evolution in death valley, california: vol. 125, pp. 1203–1223, doi:10.1130/B30789.1.

Mahon, R. C., Dehler, C. M., Link, P. K., Karlstrom, K. E., and Gehrels, G. E., , Geochronologic and stratigraphic constraints on the mesoproterozoic and neoproterozoic pahrump group, death valley, california: A record of the assembly, stability, and breakup of rodinia: vol. 126, pp. 652–664, doi:10.1130/B30956.1.

Mattinson, J. M., , Zircon u–pb chemical abrasion (“CA-TIMS”) method: Combined annealing and multi-step partial dissolution analysis for improved precision and accuracy of zircon ages: vol. 220, pp. 47–66, doi:10.1016/j.chemgeo.2005.03.011.

Nicholson, S. W. and Shirey, S. B., , Midcontinent rift volcanism in the lake superior region: Sr, nd, and pb isotopic evidence for a mantle plume origin: vol. 95, p. 10,851, doi:10.1029/JB095iB07p10851.

Peters, B. J., Day, J. M., Greenwood, R. C., Hilton, D. R., Gibson, J., and Franchi, I. A., , Helium–oxygen–osmium isotopic and elemental constraints on the mantle sources of the deccan traps: vol. 478, pp. 245–257, doi:10.1016/j.epsl.2017.08.042.

316 Prave, A. R., , Two diamictites, two cap carbonates, two 13c excursions, two rifts: The neoproterozoic
317 kingston peak formation, death valley, california: vol. 27, p. 339,
318 doi:10.1130/0091-7613(1999)027<0339:TDTCCT>2.3.CO;2.

319 Richards, M. A., Duncan, R. A., and Courtillot, V. E., , Flood basalts and hot-spot tracks: Plume heads
320 and tails: vol. 246, pp. 103–107, doi:10.1126/science.246.4926.103.

321 Roberts, M. T., a, Stratigraphy and depositional environments of the crystal spring formation, southern
322 death valley region, california: p. 9.

323 Roberts, M. T., b, THE STRATIGRAPHY AND DEPOSITIONAL ENVIRONMENTS OF THE LOWER
324 PART OF THE CRYSTAL SPRING FORMATION, DEATH VALLEY, CALIFORNIA.: p. 24.

325 Schoene, B., , U–th–pb geochronology: *In* Treatise on Geochemistry, Elsevier, pp. 341–378,
326 doi:10.1016/B978-0-08-095975-7.00310-7, URL
327 https://linkinghub.elsevier.com/retrieve/pii/B9780080959757003107.

328 Schoene, B., Crowley, J. L., Condon, D. J., Schmitz, M. D., and Bowring, S. A., , Reassessing the uranium
329 decay constants for geochronology using ID-TIMS u–pb data: vol. 70, pp. 426–445,
330 doi:10.1016/j.gca.2005.09.007.

331 Shirey, S. B., , Re-os isotopic compositions of midcontinent rift system picrites: implications for plume –
332 lithosphere interaction and enriched mantle sources: vol. 34, pp. 489–503, doi:10.1139/e17-040.

333 Sleep, N. H., , Lateral flow and ponding of starting plume material: vol. 102, pp. 10,001–10,012,
334 doi:10.1029/97JB00551.

335 Smith, E. F., MacDonald, F. A., Crowley, J. L., Hodgin, E. B., and Schrag, D. P., , Tectonostratigraphic
336 evolution of the *c.* 780–730 ma beck spring dolomite: Basin formation in the core of rodinia: vol. 424,
337 pp. 213–239, doi:10.1144/SP424.6.

338 St-Onge, M. R., Van Gool, J. A. M., Garde, A. A., and Scott, D. J., , Correlation of archaean and
339 palaeoproterozoic units between northeastern canada and western greenland: constraining the
340 pre-collisional upper plate accretionary history of the trans-hudson orogen: vol. 318, pp. 193–235,
341 doi:10.1144/SP318.7.

Strickland, B. A., Wooden, J. L., Mattinson, C. G., Ushikubo, T., Miller, D. M., and Valley, J. W., , Proterozoic evolution of the mojave crustal province as preserved in the ivanpah mountains, southeastern california: vol. 224, pp. 222–241, doi:10.1016/j.precamres.2012.09.006.

Swanson-Hysell, N. L., Hoaglund, S. A., Crowley, J. L., Schmitz, M. D., Zhang, Y., and Miller, J. D., a, Rapid emplacement of massive duluth complex intrusions within the north american midcontinent rift: vol. 49, pp. 185–189, doi:10.1130/G47873.1.

Swanson-Hysell, N. L., Ramezani, J., Fairchild, L. M., and Rose, I. R., b, Failed rifting and fast drifting: Midcontinent rift development, laurentia's rapid motion and the driver of grenvillian orogenesis: vol. 131, pp. 913–940, doi:10.1130/B31944.1.

Tanton, L. T. E. and Hager, B. H., , Melt intrusion as a trigger for lithospheric foundering and the eruption of the siberian flood basalts: vol. 27, pp. 3937–3940, doi:10.1029/2000GL011751.

Tauxe, L., Shaar, R., Jonestrask, L., Swanson-Hysell, N. L., Minnett, R., Koppers, A. A. P., Constable, C. G., Jarboe, N., Gaastra, K., and Fairchild, L., , PmagPy: Software package for paleomagnetic data analysis and a bridge to the magnetics information consortium (MagIC) database: vol. 17, pp. 2450–2463, doi:10.1002/2016GC006307.

Tsekhmistrenko, M., Sigloch, K., Hosseini, K., and Barruol, G., , A tree of indo-african mantle plumes imaged by seismic tomography: vol. 14, pp. 612–619, doi:10.1038/s41561-021-00762-9.

van der Lee, S., Regenauer-Lieb, K., and Yuen, D. A., , The role of water in connecting past and future episodes of subduction: vol. 273, pp. 15–27, doi:10.1016/j.epsl.2008.04.041.

Vermeesch, P., , IsoplotR: A free and open toolbox for geochronology: vol. 9, pp. 1479–1493, doi:10.1016/j.gsf.2018.04.001.

Whitmeyer, S. J. and Karlstrom, K. E., , Tectonic model for the proterozoic growth of north america: p. 40.

Wright, L., , Talc deposits of the southern death valley-kingston range region, california: p. 88.

Wrucke, C. T., , Geologic map of the warm spring canyon area, death valley national park, inyo county, california: Series: Scientific Investigations Map.

Figures

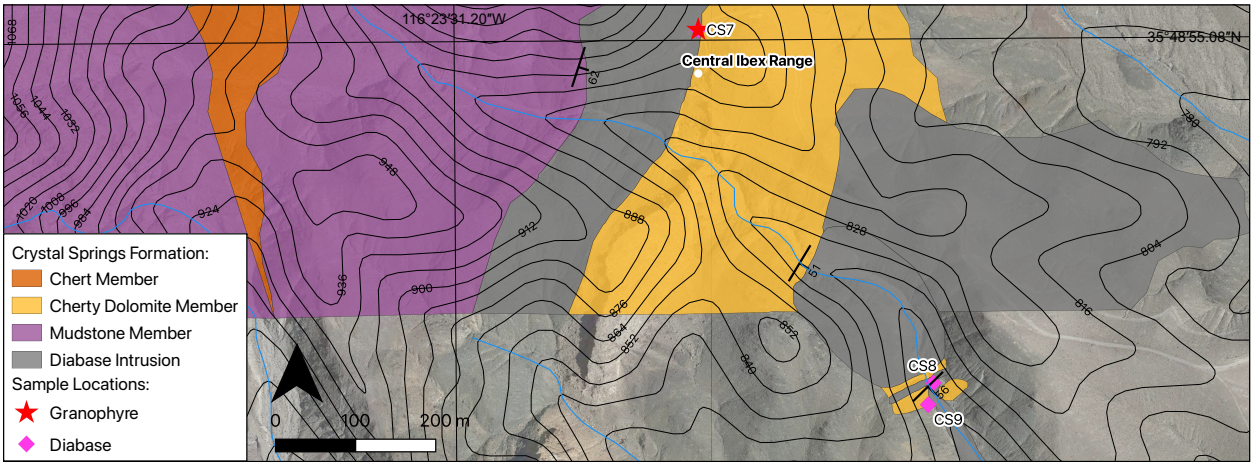

Figure 15

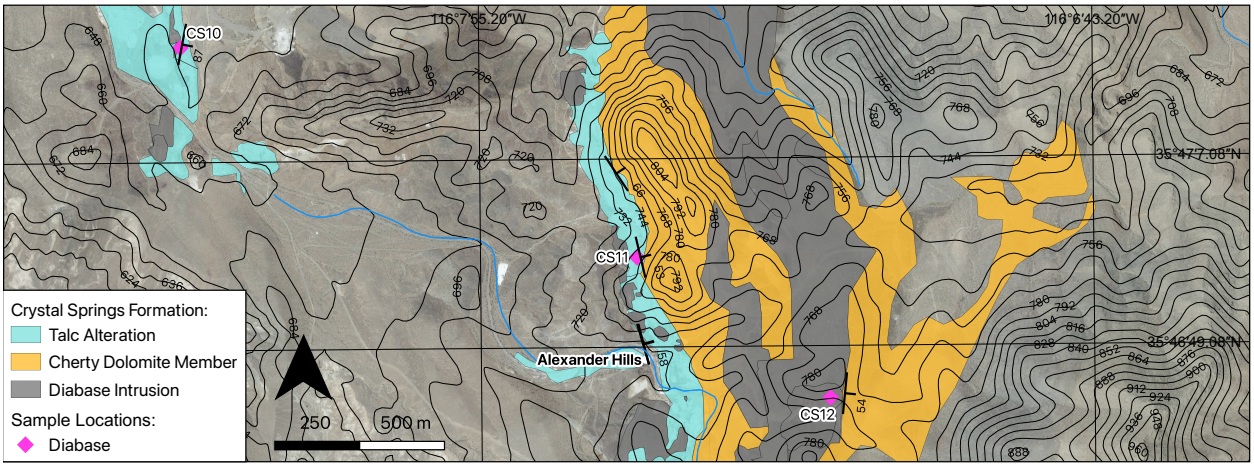

Figure 16. Geologic map of the Alexander Hills depicting exposed units of the Crystal Springs Formation and paleomagnetic sample sites CS10-12 and exposed units of the Crystal Springs Formation. Within the field area the Dolomite Member has been metamorphosed to talc from sill intrusion.

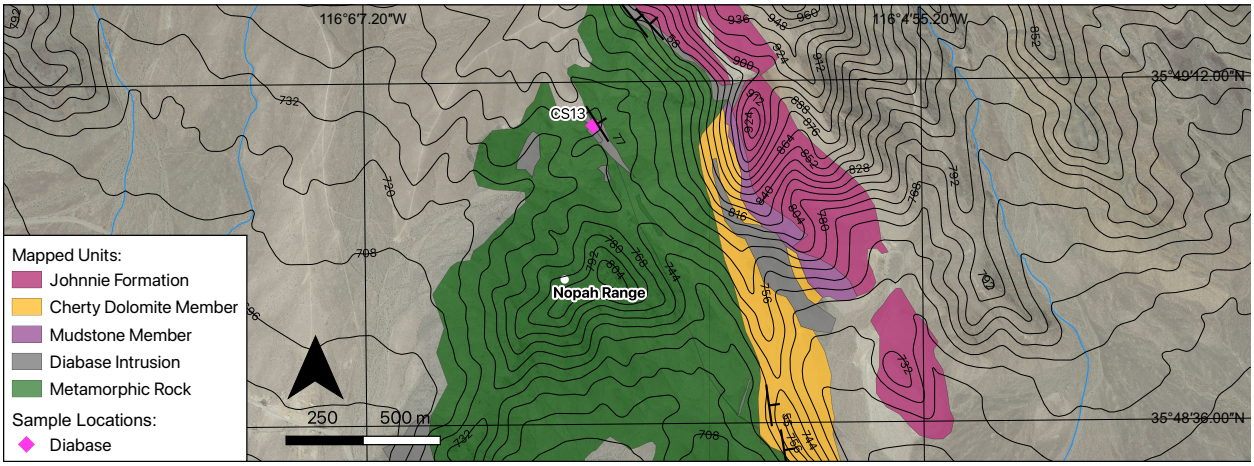

Figure 17. Geologic map of the Nopah Range highlighting paleomagnetic site CS13 and exposures of Crystal Springs Formation and the unconformably overlying Johnnie Formation. The unconformity between the formations spans >300 Ma and represents the erosion of Horse Thief Springs, Beck Springs Dolomite, Kingston Peak and Noonday Formations.

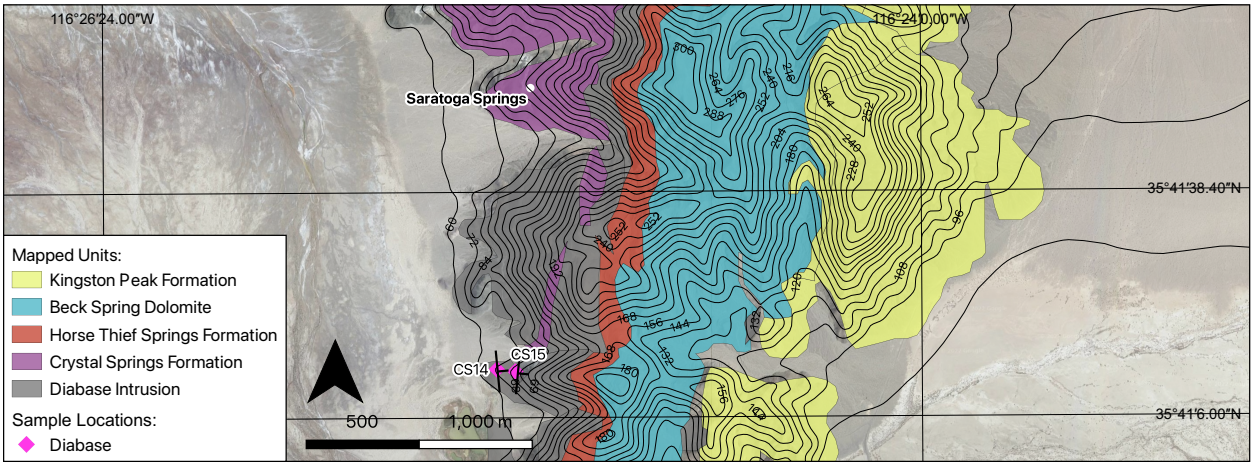

Figure 18. Geologic map of southern Saratoga Hills depicting paleomagnetic sites CS14 and CS15 and lithological units of the Pahrump group. Within the Pahrump Group, Crystal Springs sits atop metamorphosed basement rock and is overlaid unconformably (∼300 Ma) by Horse Thief Springs and Beck Spring Dolomite. A subsequent unconformity separates these units from the overlying Kingston Peak Formation.

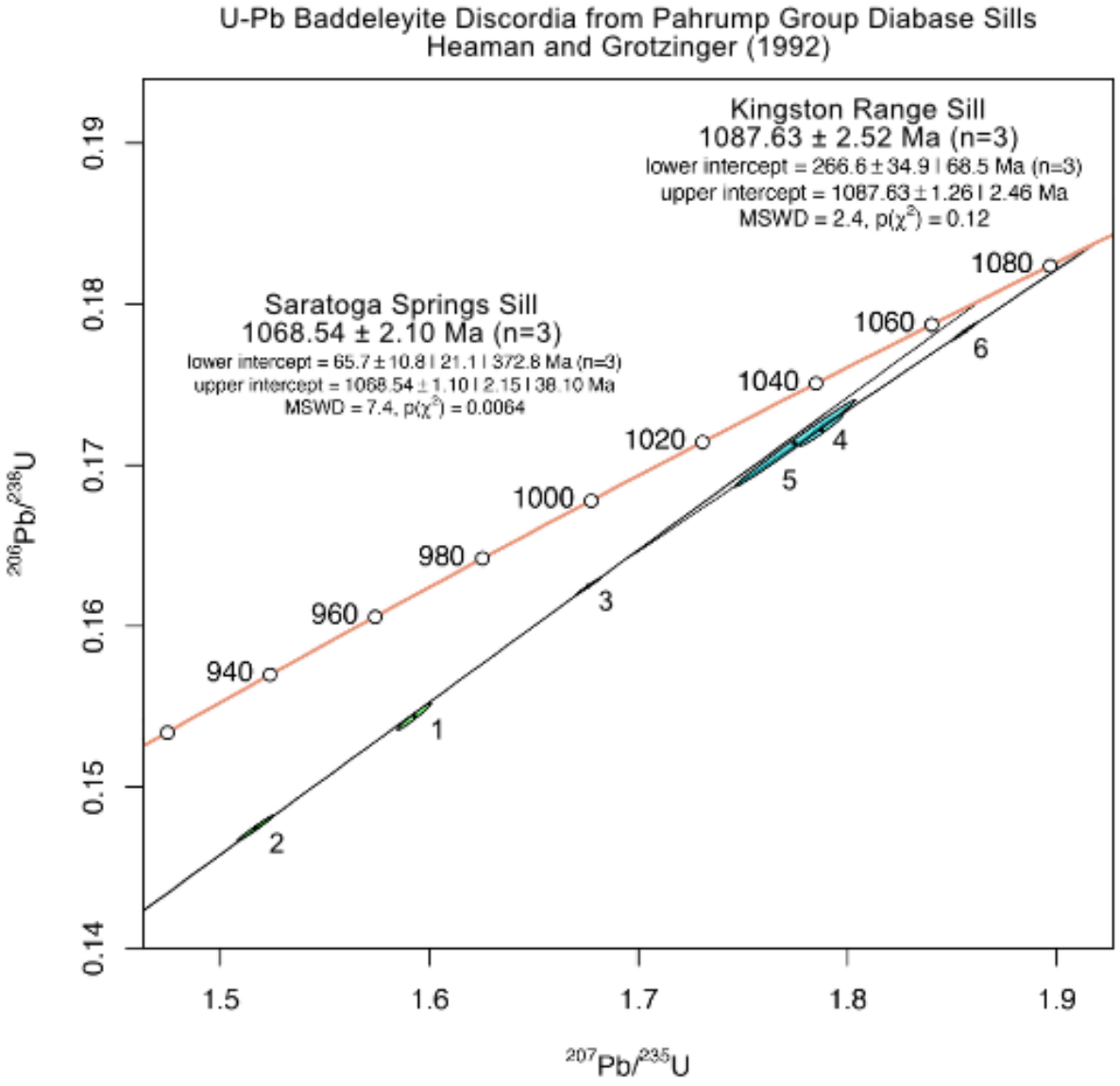

Figure 19. Concordia comparison between concordant 1097.57±.26 Ma Warm Spring Canyon felsic segregations samples obtained in this study and previously dated discordant Death Valley baddeleyite. Upper intercepts from 1992 study of Saratoga Springs Sill and Kingston Range sill are 1069 ±3 Ma and 1087 ±3 Ma, respectively. (Heaman and Grotzinger)

U-Th-Pb isotopic data

	Compositional Parameters						Radiogenic Isotope Ratios								Isotopic Dates (Ma)					
Sample	Th/U	206Pb* x10-13 mol	mol % 206Pb*	Pb*/Pbc	Pbc (pg)	206Pb/204Pb	208Pb/206Pb	207Pb/206Pb	% err	207Pb/235U	% err	206Pb/238U	% err	corr. coef.	207Pb/206Pb	±	207Pb/235U	±	206Pb/238U	±
(a)	(b)	(c)	(c)	(c)	(c)	(d)	(e)	(e)	(f)	(e)	(f)	(e)	(f)		(g)	(f)	(g)	(f)	(g)	(f)
MM21-CS4-NSH																				
z1	1.210	0.5239	99.28%	50	0.31	2518	0.366	0.076288	0.141	1.953293	0.209	0.185783	0.089	0.852	1101.74	2.82	1099.58	1.40	1098.49	0.90
z2	0.997	1.1020	99.61%	88	0.36	4625	0.302	0.076253	0.101	1.952261	0.173	0.185771	0.083	0.927	1100.81	2.02	1099.22	1.16	1098.42	0.83
z3	1.442	0.8278	99.73%	137	0.19	6592	0.437	0.076211	0.094	1.950890	0.169	0.185741	0.084	0.939	1099.72	1.89	1098.75	1.14	1098.26	0.85
z4	0.898	0.8338	98.29%	19	1.21	1045	0.272	0.076202	0.225	1.951508	0.307	0.185822	0.147	0.723	1099.48	4.51	1098.97	2.06	1098.70	1.48
z5	0.734	1.3086	99.77%	142	0.25	7972	0.222	0.076254	0.088	1.952504	0.162	0.185790	0.081	0.954	1100.85	1.76	1099.31	1.09	1098.53	0.82
z6	1.096	0.5938	98.33%	21	0.84	1077	0.332	0.076287	0.253	1.953267	0.315	0.185782	0.104	0.700	1101.72	5.06	1099.57	2.11	1098.48	1.05
z7	0.975	1.1875	99.78%	152	0.22	8053	0.295	0.076248	0.089	1.951466	0.164	0.185706	0.081	0.958	1100.69	1.78	1098.95	1.10	1098.07	0.82
z8	1.259	0.7734	99.64%	100	0.23	4998	0.381	0.076250	0.105	1.951563	0.176	0.185711	0.083	0.926	1100.74	2.09	1098.98	1.18	1098.10	0.83
z9	0.865	1.6666	99.85%	227	0.20	12310	0.262	0.076280	0.083	1.953349	0.158	0.185806	0.080	0.967	1101.54	1.66	1099.60	1.06	1098.62	0.81

(a) z1, z2 etc. are labels for single zircon grains or fragments annealed and chemically abraded after Mattinson (2005).

(b) Model Th/U ratio iteratively calculated from the radiogenic 208Pb/206Pb ratio and 206Pb/238U age.

(c) Pb* and Pbc represent radiogenic and common Pb, respectively; mol % 206Pb* with respect to radiogenic, blank and initial common Pb.

(d) Measured ratio corrected for spike and fractionation only. Fractionation estimated at 0.17 +/- 0.036 %/a.m.u. for Daly analyses, based on laboratory compilation of analyses using ET2535 tracer.

(e) Corrected for fractionation, spike, and common Pb; up to 1 pg of common Pb was assumed to be procedural blank: 206Pb/204Pb = 18.042 ± 0.61%; 207Pb/204Pb = 15.537 ± 0.52%; 208Pb/204Pb = 37.686 ± 0.63% (all uncertainties 1-sigma). Excess over blank was assigned to initial common Pb, using the Stacey and Kramers (1975) two-stage Pb isotope evolution model at the nominal sample age.

(f) Errors are 2-sigma, propagated using the algorithms of Schmitz and Schoene (2007).

(g) Calculations are based on the decay constants of Jaffey et al. (1971). 206Pb/238U and 207Pb/206Pb ages corrected for initial disequilibrium in 230Th/238U using Th/U [magma] = 3 ± 1.

(h) Corrected for fractionation, spike, and blank Pb only.

Figure 20. U-Th-Pb zircon data from felsic segregations acquired at site CS4. Note: Ages in above table are calculated using decay constants by (Hiess et al.)